Electronic Supplementary Material (ESI) for RSC Advances.

Supporting Information

Multiple target chemosensor: a fluorescent sensor for Zn(II) and Al(III) and chromogenic sensor for Fe(II) and Fe(III)

Yong Sung Kim, Gyeong Jin Park, Jae Jun Lee, Sun Young Lee, Seong Youl Lee, Cheal Kim*

Department of Fine Chemistry and Department of Interdisciplinary Bio IT Materials, Seoul National University of Science and Technology, Seoul 139-743, Korea. Fax: +82-2-973-9149; Tel: +82-2-970-6693; E-mail:chealkim@seoultech.ac.kr

Table S1. Determination of Zn(II) in Tap water

Sample	Zn(II) added (μmol/L)	Zn(II) found (μmol/L)	Recovery (%)	R.S.D. (n = 3) (%)
Tap water	0.00	0.00	-	-
	110.00	113.11	102.8	0.8

Conditions: [**1**] = 10 μmol/L in DMF-buffer solution (95:5, v/v, 10 mM, bis-tris, pH 7.0).

Table S2. Determination of Fe(III) in water samples

Sample	Fe(III) added (μmol/L)	Fe(III) found (μmol/L)	Recovery (%)	R.S.D. (n = 3) (%)
Tap water	0.00	0.00	-	-
	15.00	14.58	97.2	3.1
Water sample[a]	0.00	0.00	-	-
	15.00	14.52	96.8	1.8

[a] Synthesized by deionized water, 6.00 μmol/L Zn(II), 10 μmol/L Cd(II), Pb(II), Na(I), K(I), Ca(II), Mg(II). Conditions: [**1**] = 10 μmol/L in 10 mM MeOH-bis-tris buffer solution (9:1, pH 7.0).

(a)

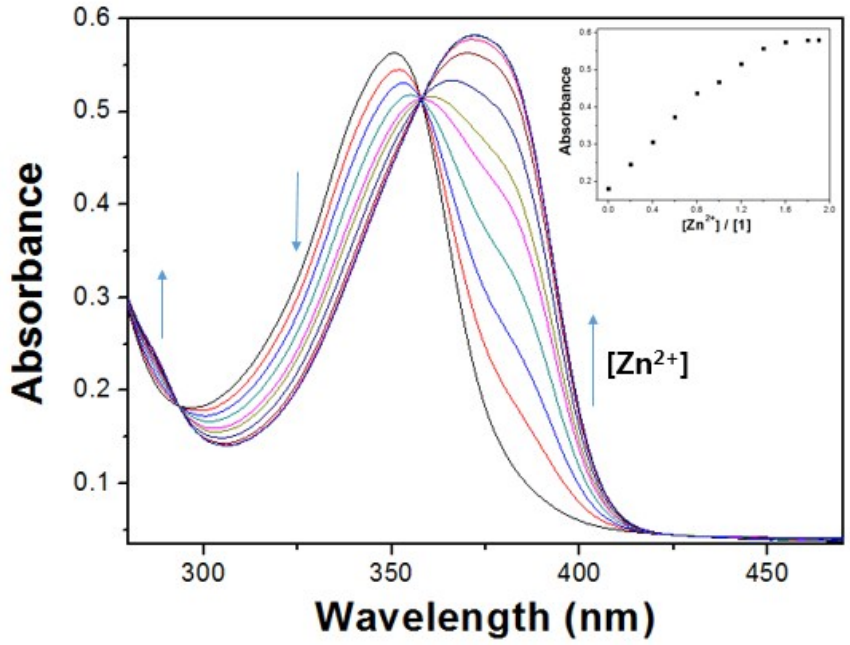

(b)

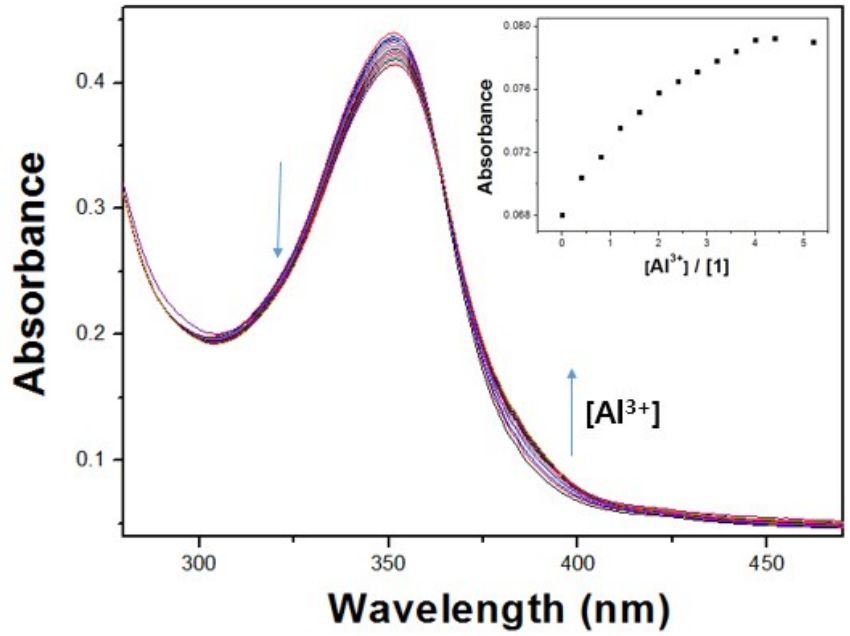

Figure S1. (a) UV-vis spectral changes of **1** (10 μM) after addition of zinc ions (0, 0.2, 0.4, 0.6, 0.8, 1.0, 1.2, 1.4, 1.6, 1.8, and 1.9 equiv) in DMF. Inset: Plot of the UV-vis absorbance at 375 nm as a function of Zn^{2+} concentration. (b) UV-vis spectral changes of **1** (10 μM) after addition of aluminium ions (0, 0.4, 0.8, 1.2, 1.6, 2.0, 2.4, 2.8, 3.2, 3.6, 4.0, 4.4 and 5.2 equiv) in DMF. Inset: Plot of the UV-vis absorbance at 400 nm as a function of Al^{3+} concentration.

(a)

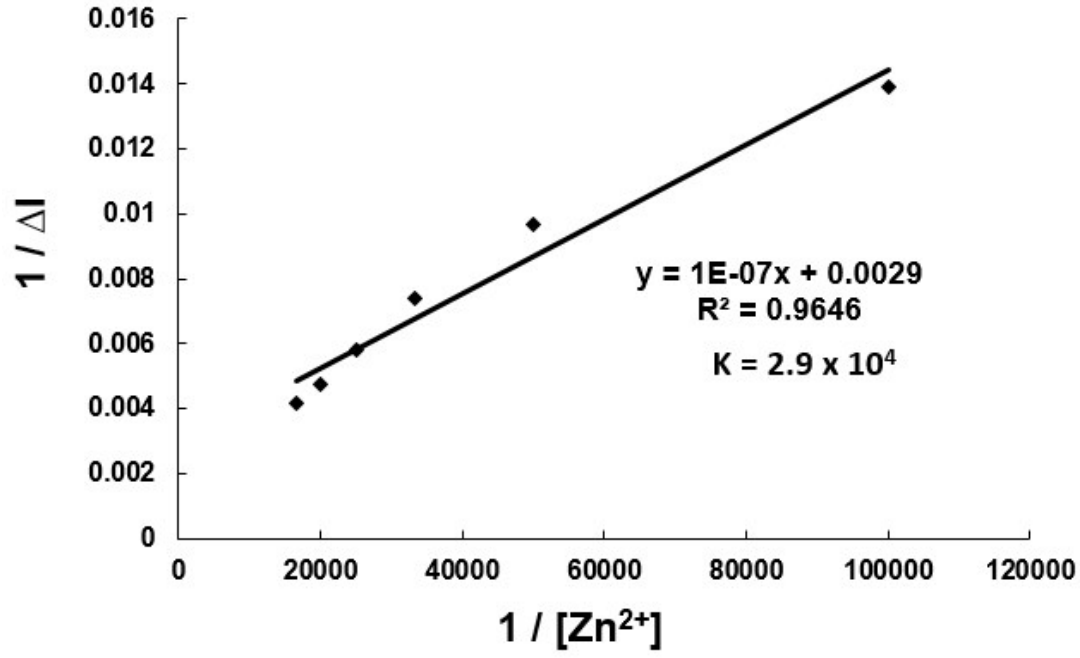

(b)

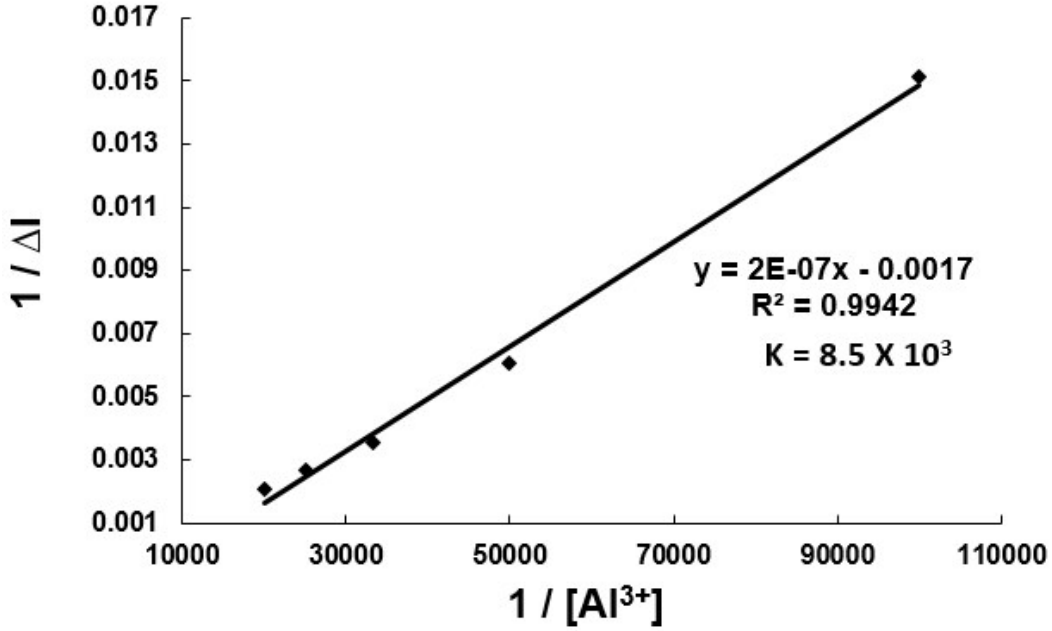

Figure S2. (a) Benesi-Hildebrand equation plot (fluorescence intensity at 448 nm) of **1**, assuming 1:1 stoichiometry for association between **1** and Zn^{2+}. (b) Benesi-Hildebrand equation plot (fluorescence intensity at 418 nm) of **1**, assuming 1:1 stoichiometry for association between **1** and Al^{3+}.

(a)

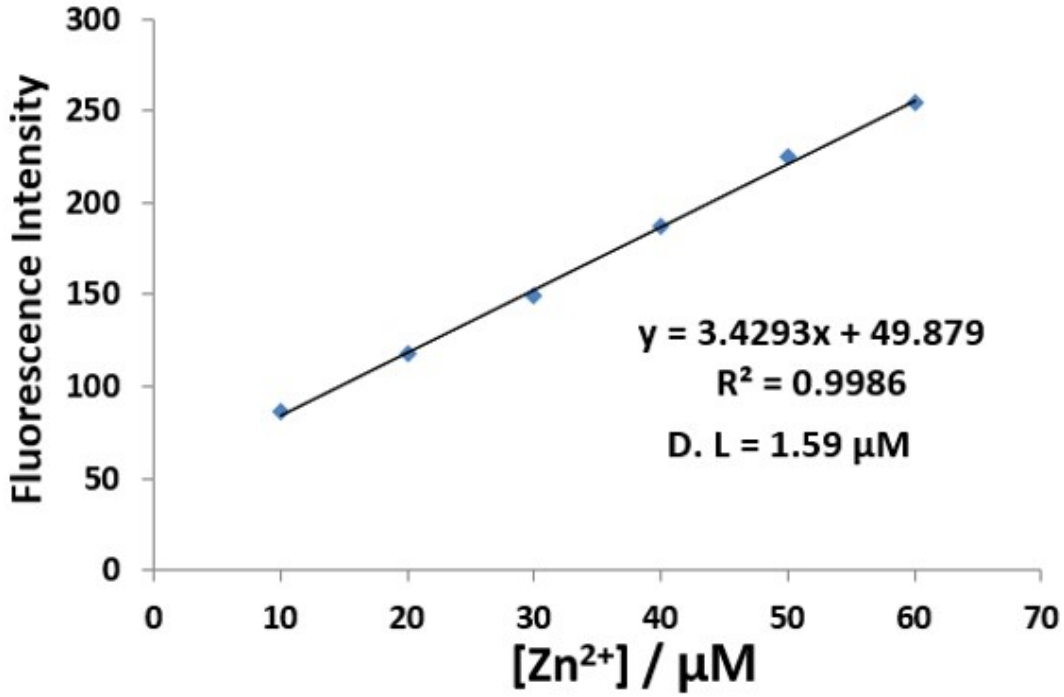

(b)

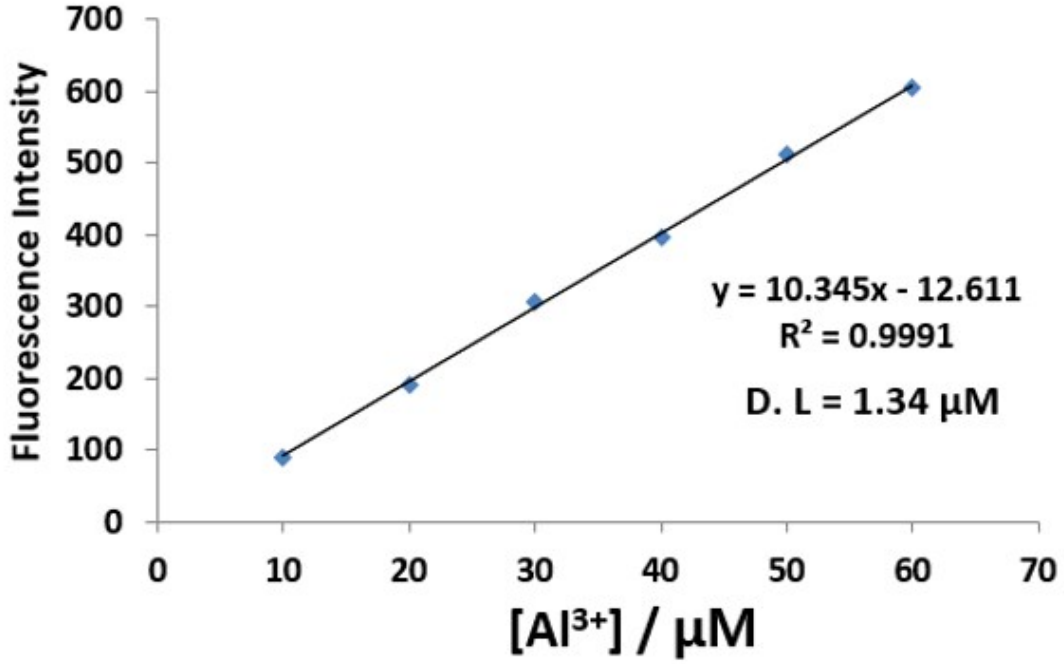

Figure S3. (a) Detection limit of **1** (10 μM) for Zn^{2+} through change of absorbance intensity (fluorescence intensity at 448 nm). (b) Detection limit of **1** (10 μM) for Al^{3+} through change of absorbance intensity (fluorescence intensity at 418 nm).

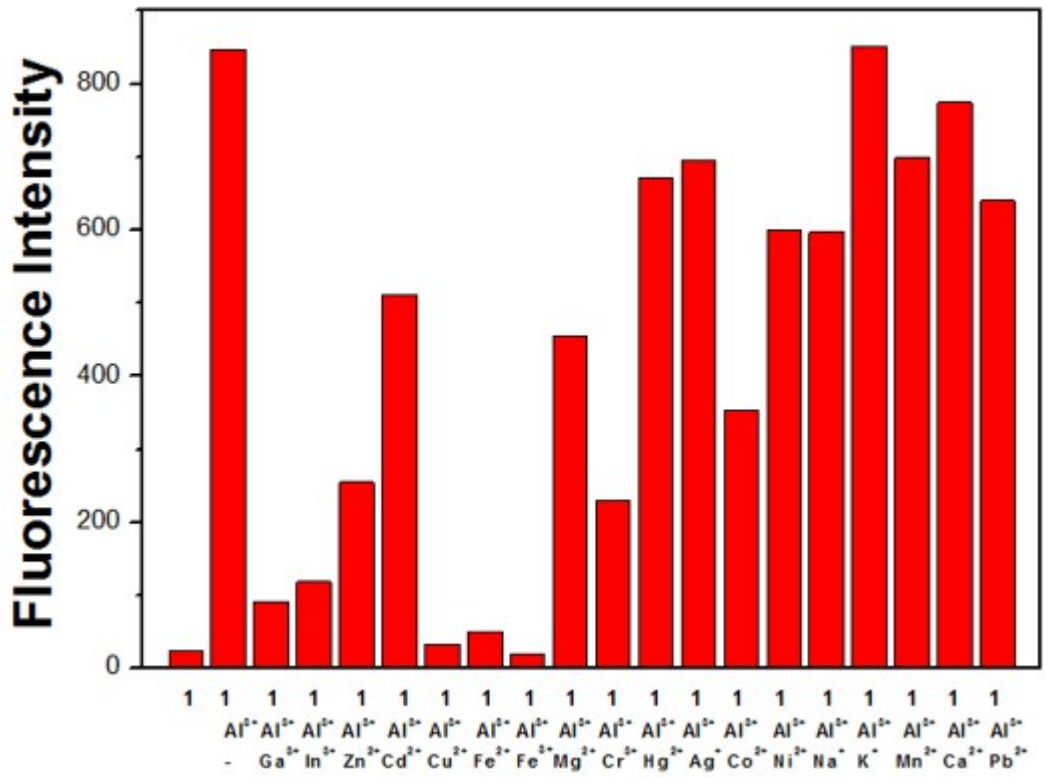

Figure S4. Effect of competitive metal ions (10 μM) on the interaction between **1** (110 μM) and Al^{3+} ion (110 μM) in DMF (λ_{ex} = 355 nm and λ_{em} = 456 nm).

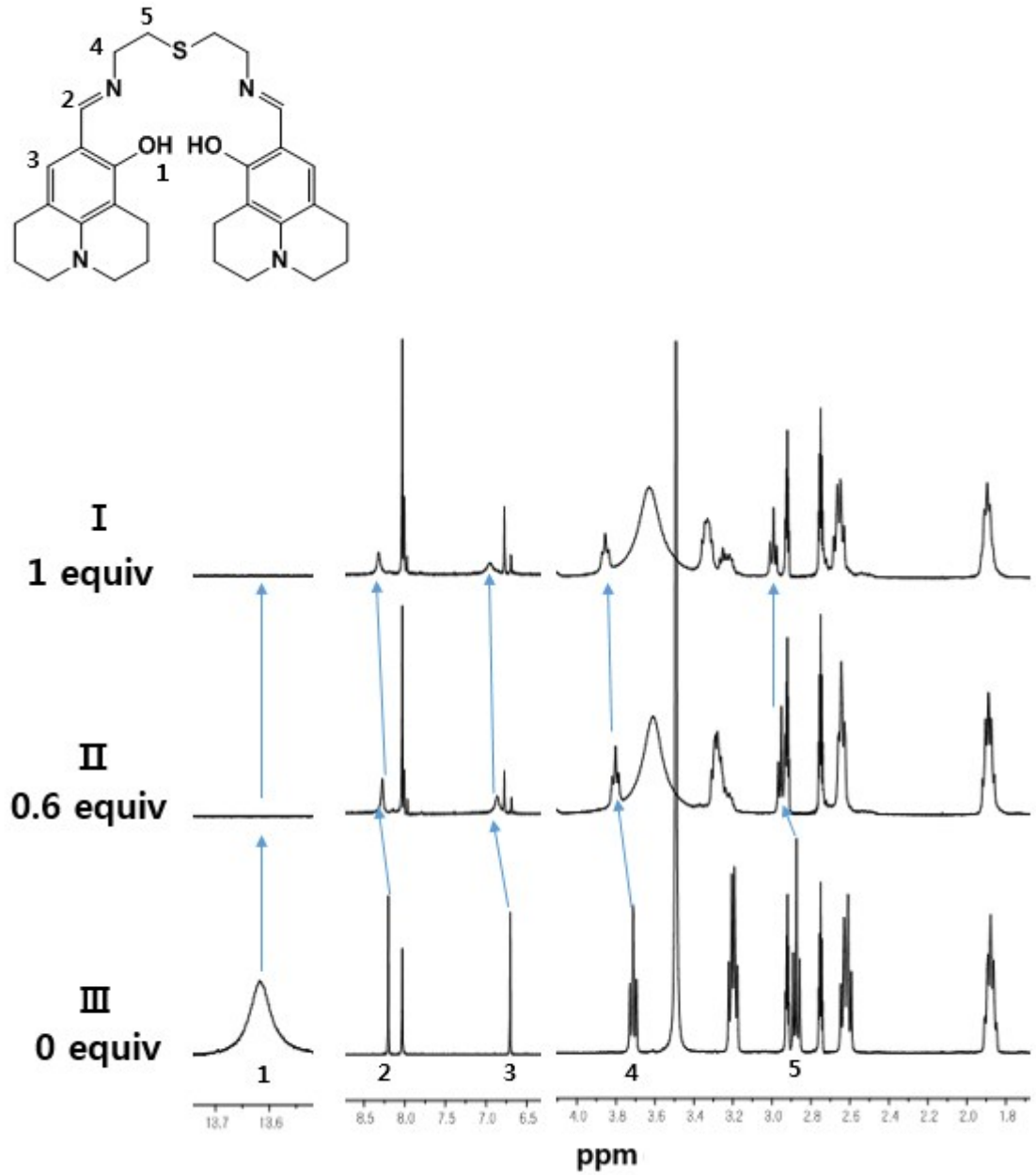

Figure S5. ^{1}H NMR titration of **1** with Al^{3+} in DMF-d_7: (a) only **1**; (b) **1**+Al^{3+} (0.6 equiv); (c) **1**+ Al^{3+} (1 equiv).

(a)

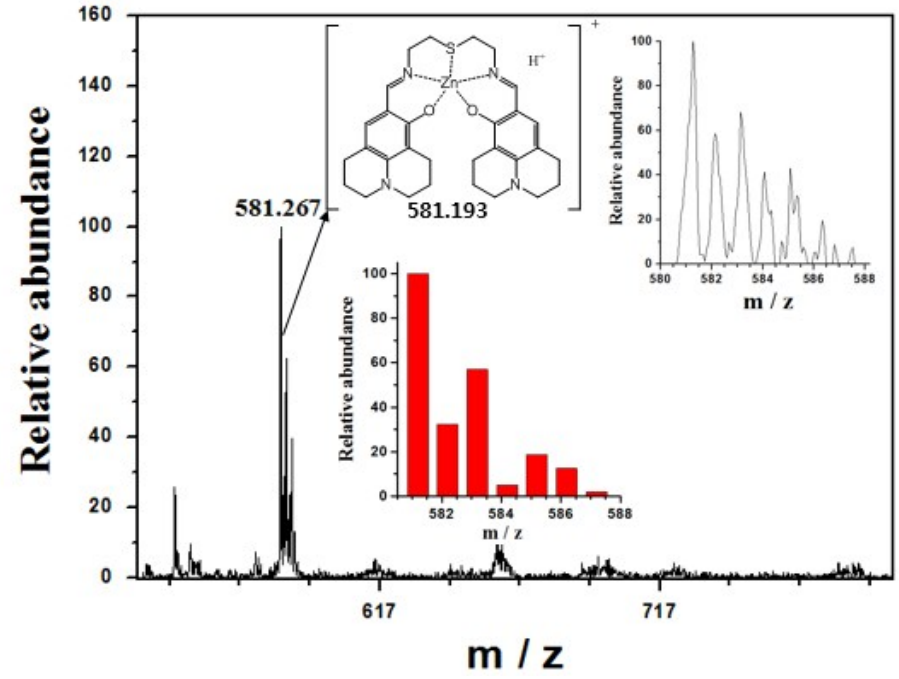

(b)

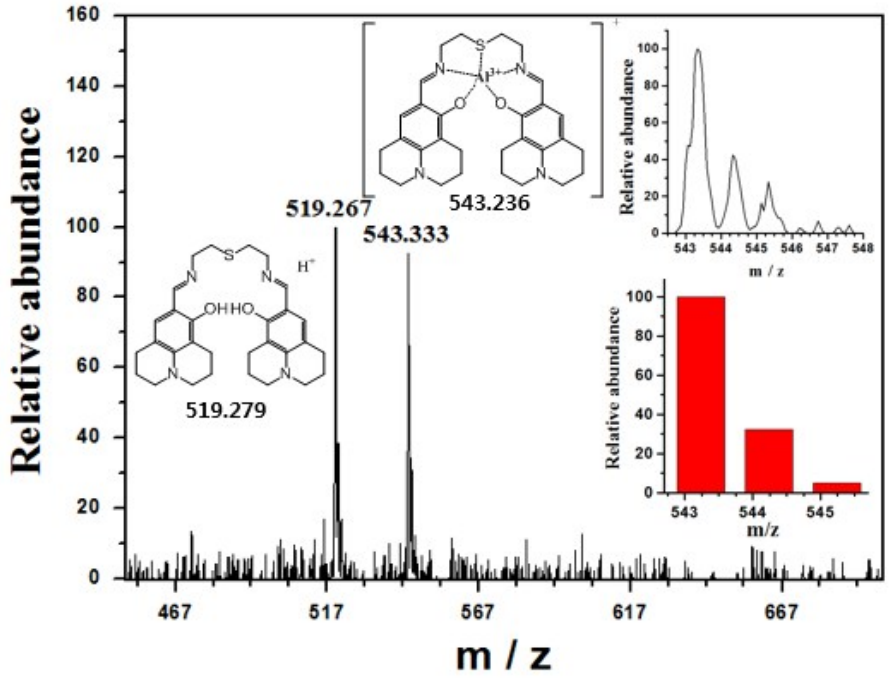

Figure S6. (a) Positive-ion electrospray ionization mass spectrum of **1** (100 μM) upon addition of 1 equiv of $Zn(NO_3)_2$. (b) Positive-ion electrospray ionization mass spectrum of **1** (100 μM) upon addition of 1 equiv of $Al(NO_3)_3$.

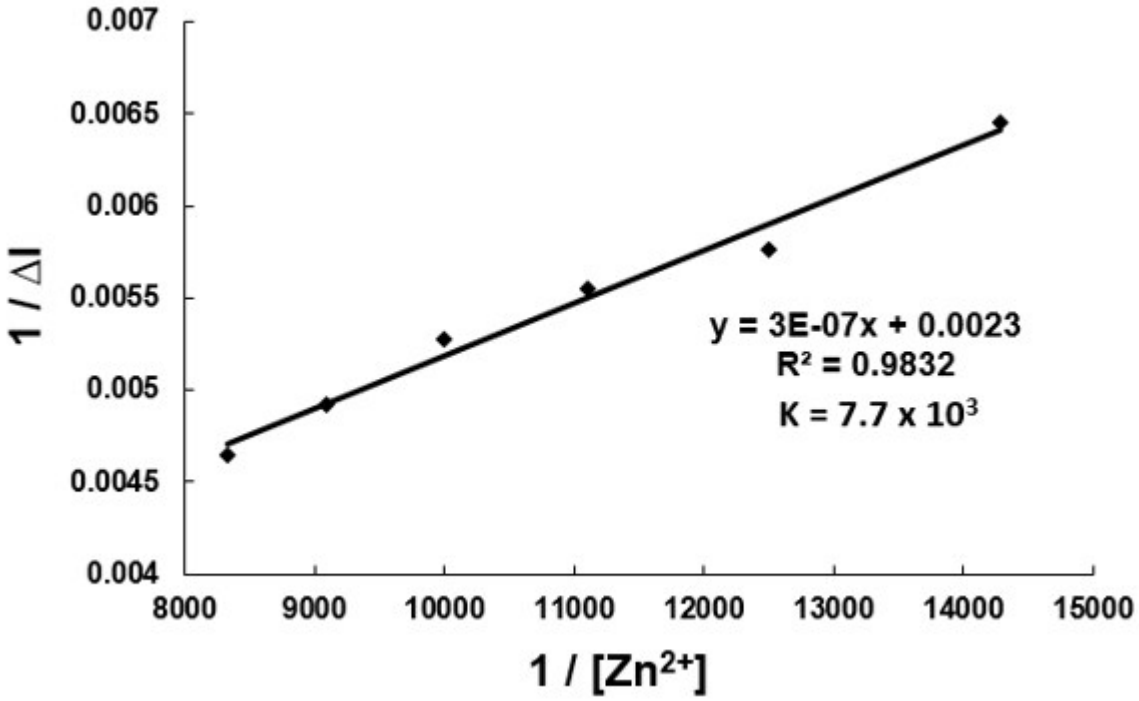

Figure S7. Benesi-Hildebrand equation plot (fluorescence intensity at 446 nm) of **1**, assuming 1:1 stoichiometry for association between **1** and Zn^{2+}.

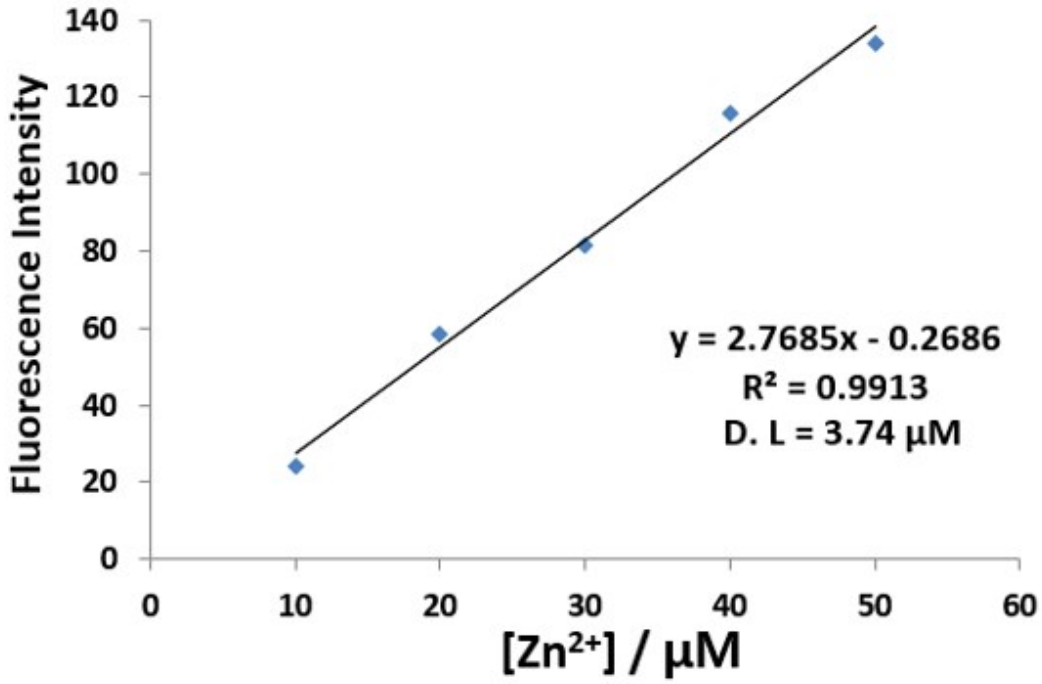

Figure S8. Detection limit of **1** (10 μM) for Zn^{2+} through change of fluorescence intensity (fluorescence intensity at 446 nm).

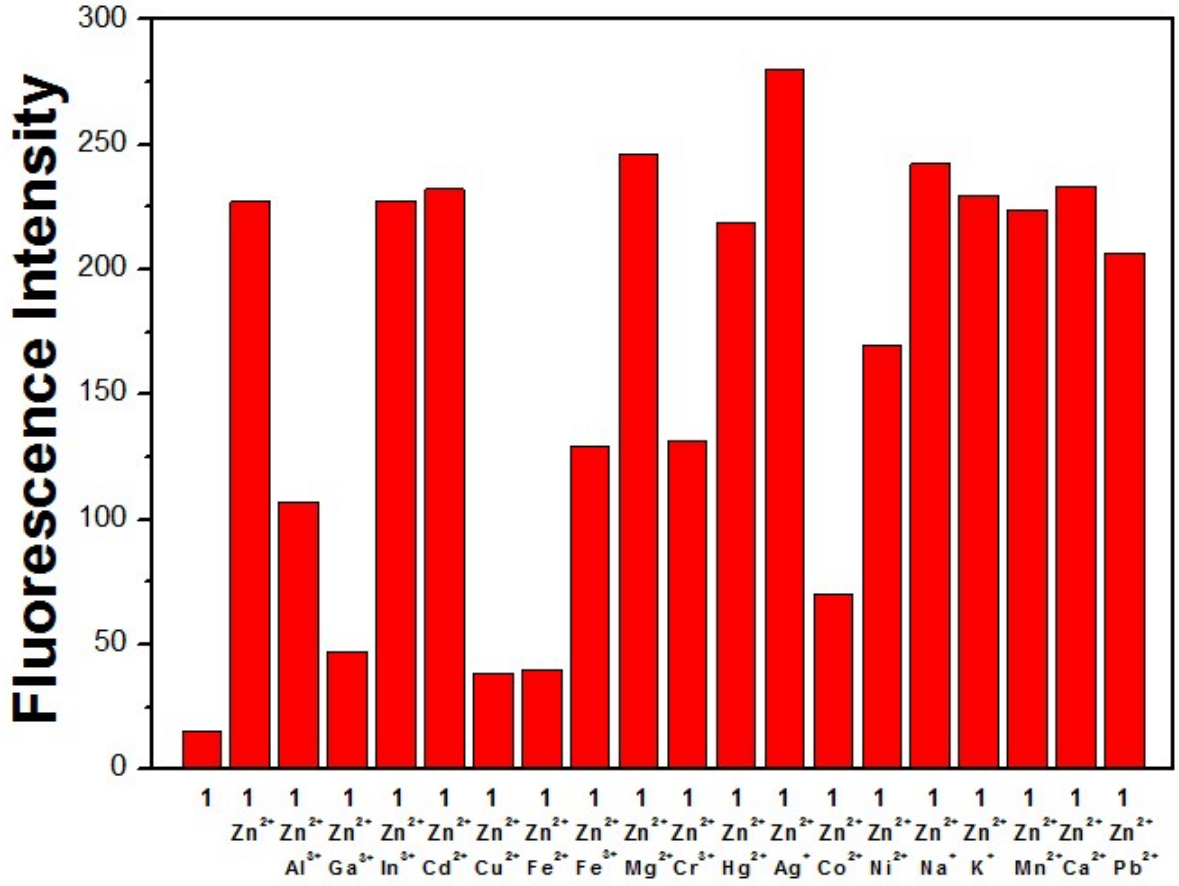

Figure S9. Effect of competitive metal ions (12 equiv) on the interaction between **1** (10 μM) and Zn^{2+} ion (120 μM) in DMF-buffer solution (95:5, v/v, 10 mM, bis-tris, pH 7.0) (λ_{ex} = 355 nm and λ_{em} = 456 nm).

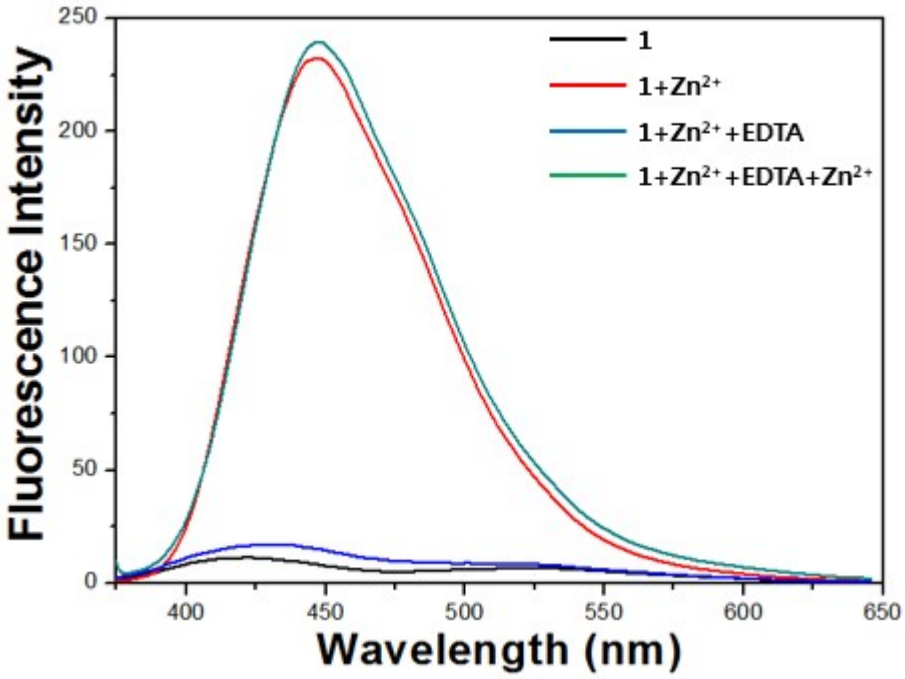

Figure S10. Fluorescence spectra of sensor **1** in the presence of Zn^{2+} ion and EDTA in DMF-buffer solution (95:5, v/v, 10 mM, bis-tris, pH 7.0). λ_{ex} = 355 nm and λ_{em} = 456 nm.

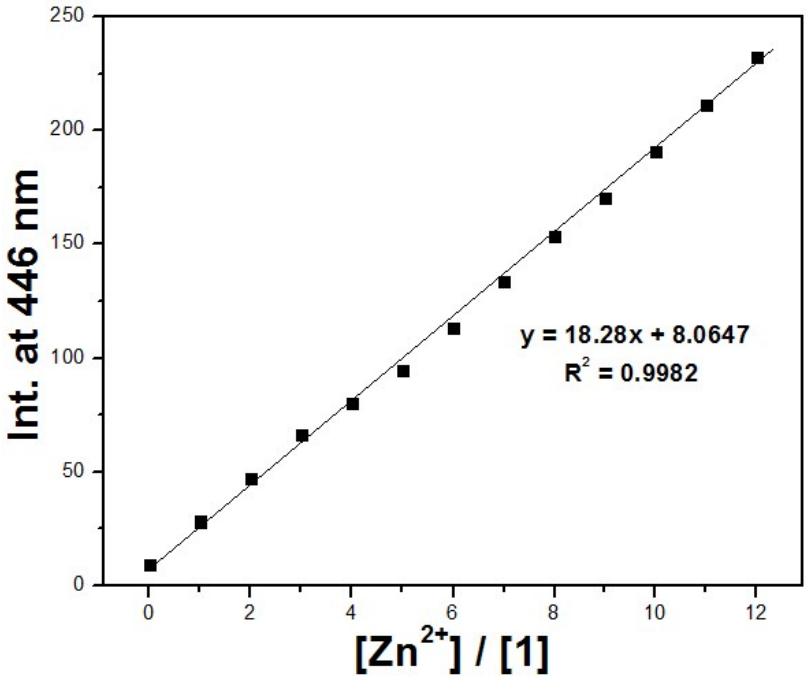

Figure S11. Fluorescence intensity (at 446 nm) of **1** as a function of Zn(II) concentration. [**1**] = 10 μM, [Zn(II)] = 0-120.00 μM; Conditions: the sample was conducted in DMF-buffer solution (95:5, v/v, 10 mM, bis-tris, pH 7.0). λ_{ex} = 355 nm and λ_{em} = 456 nm.

(a)

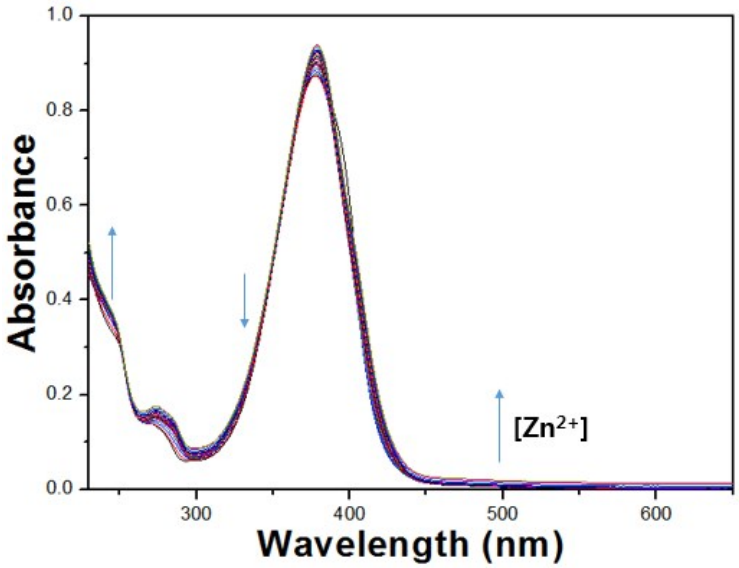

(b)

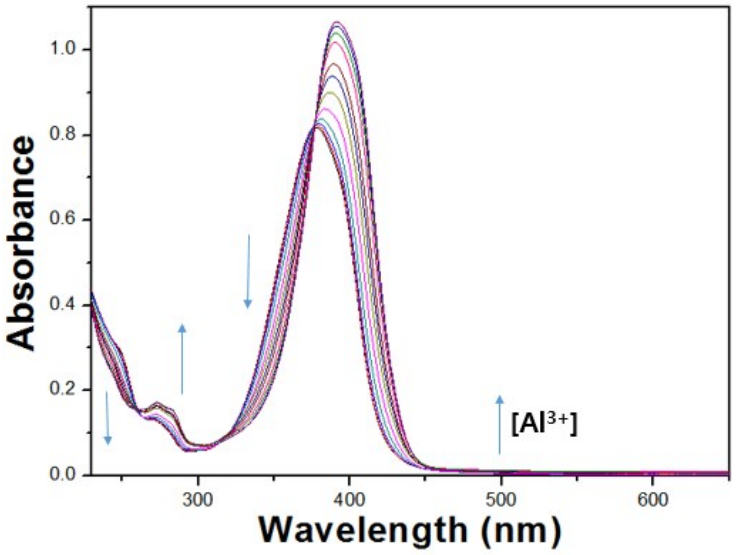

Figure S12. (a) UV-vis titration of **1** (10 μM) with Zn^{2+} (0-1.9 equiv) in MeOH-buffer solution (9:1, v/v, 10 mM, bis-tris, pH 7.0). (b) UV-vis titration of **1** (10 μM) with Al^{3+} (0-1.2 equiv) in MeOH-buffer solution (9:1, v/v, 10 mM, bis-tris, pH 7.0).

(a)

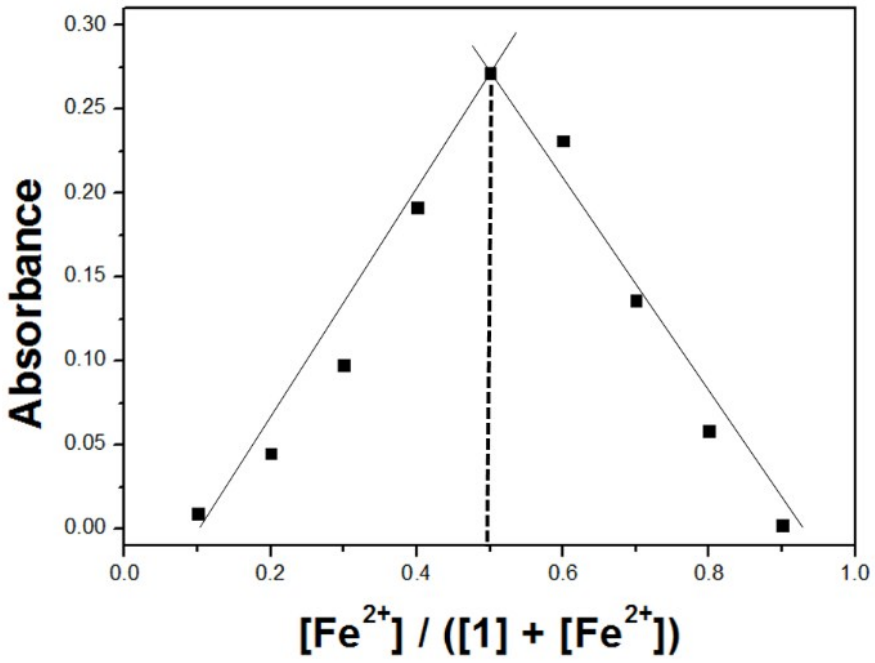

(b)

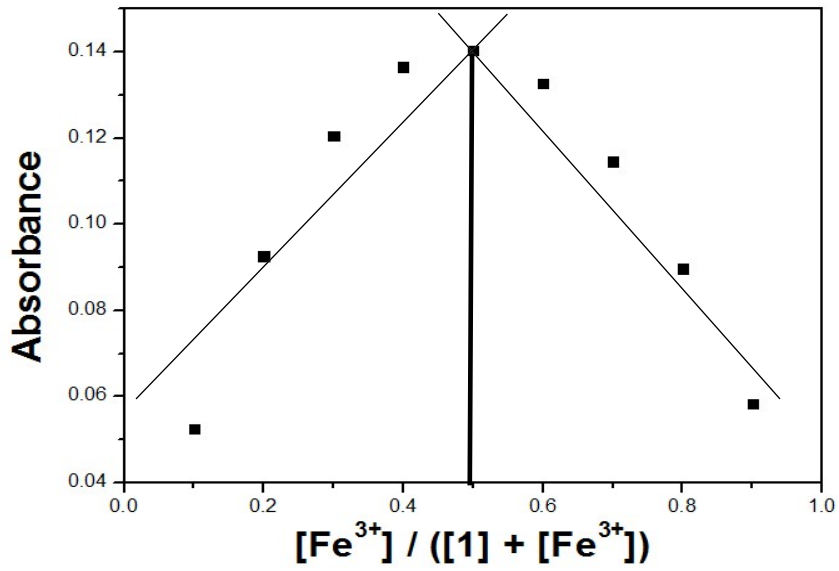

Figure S13. (a) Job plot of **1** and Fe^{2+} in MeOH-buffer solution (9:1, v/v, 10 mM, bis-tris, pH 7.0). The total concentration of **1** and Fe^{2+} was 40 μM (absorbance at 461 nm). (a) Job plot of **1** and Fe^{3+} in MeOH-buffer solution (9:1, v/v, 10 mM, bis-tris, pH 7.0). The total concentration of **1** and Fe^{3+} was 40 μM (absorbance at 450 nm).

(a)

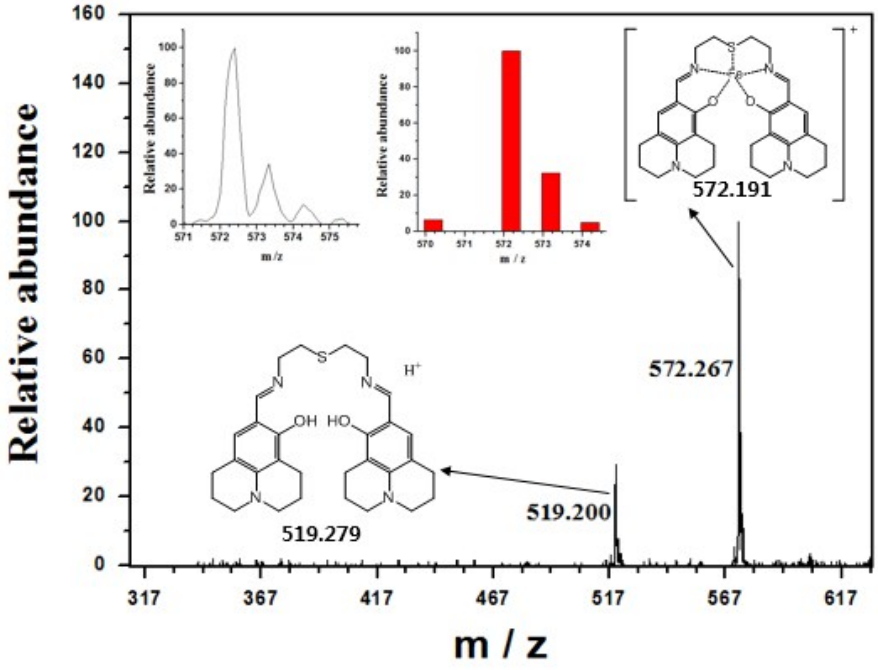

(b)

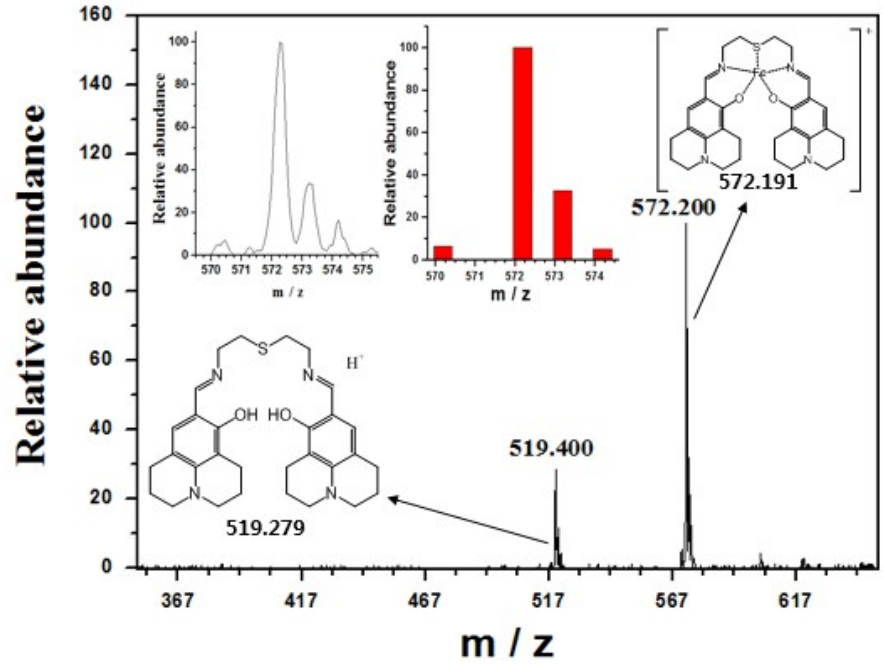

Figure S14. (a) Positive-ion electrospray ionization mass spectrum of **1** (100 μM) upon addition of 1 equiv of $Fe(NO_3)_3$. (b) Positive-ion electrospray ionization mass spectrum of **1** (100 μM) upon addition of 1 equiv of $Fe(ClO_4)_2$.

(a)

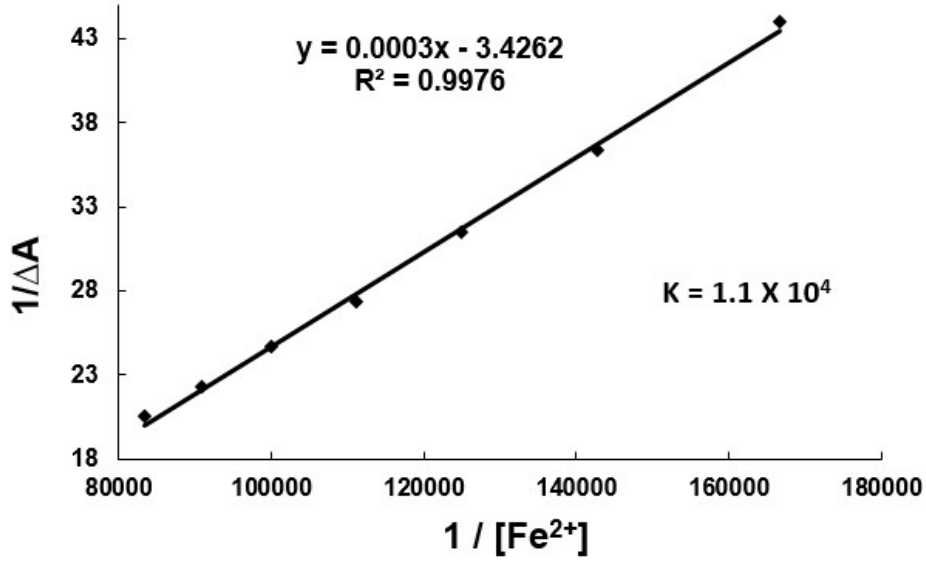

(b)

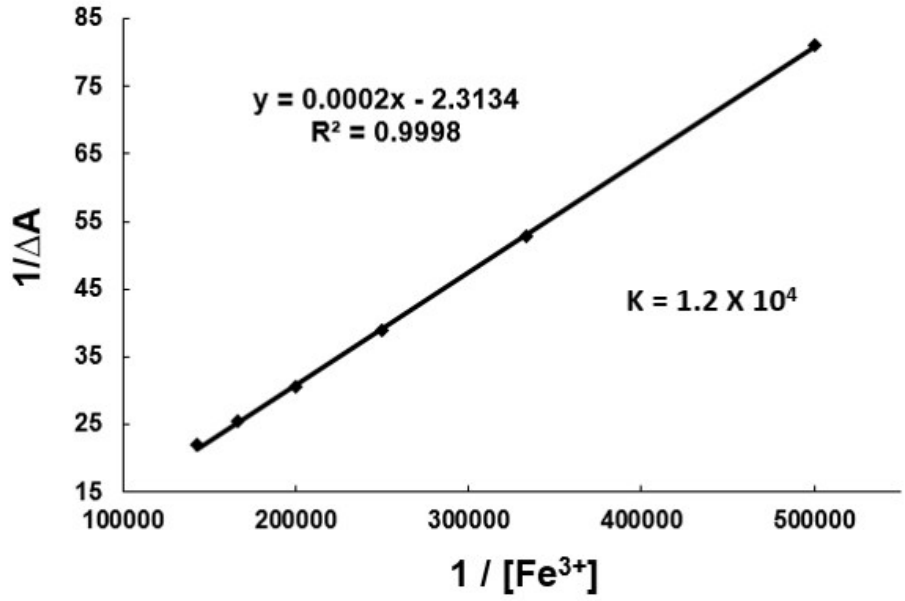

Figure S15. (a) Benesi-Hildebrand plot (absorbance at 457 nm) of **1**, assuming 1:1 stoichiometry for association between **1** and Fe^{2+}. (b) Benesi-Hildebrand plot (absorbance at 457 nm) of **1**, assuming 1:1 stoichiometry for association between **1** and Fe^{3+}.

(a)

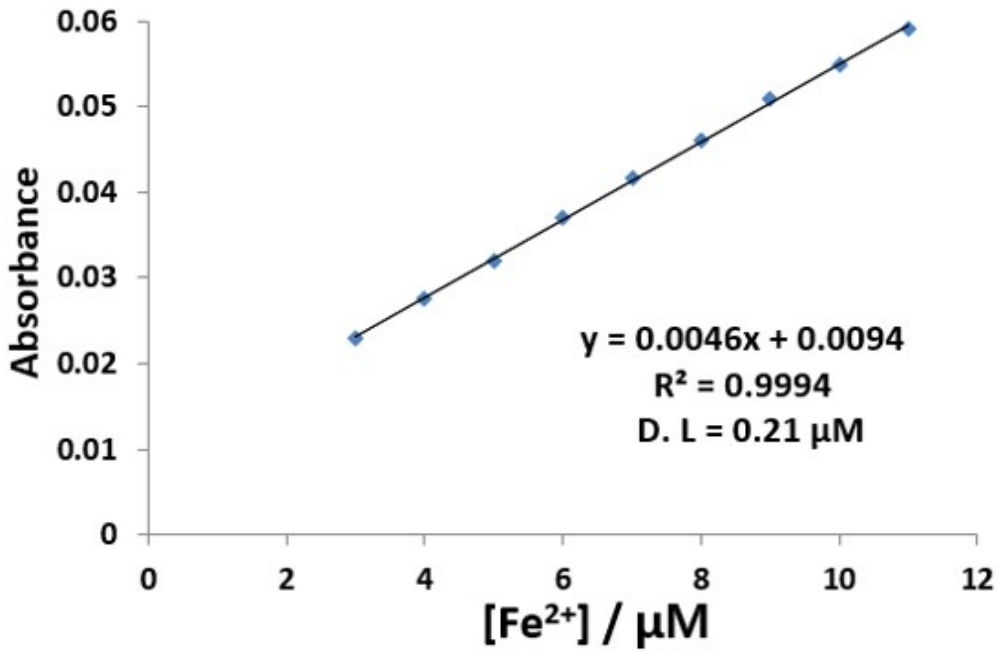

(b)

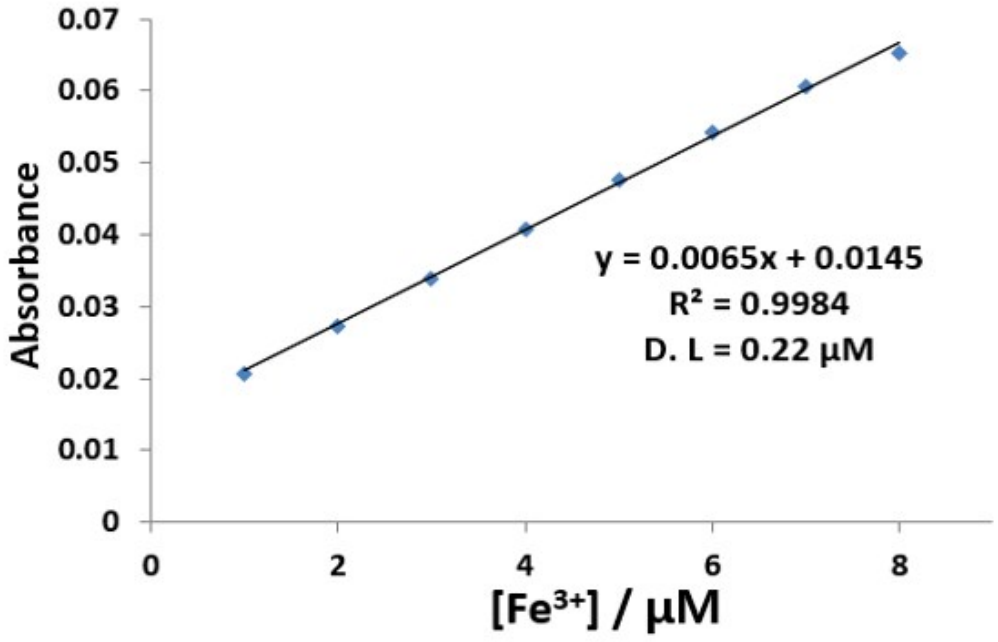

Figure S16. (a) Detection limit of **1** (10 μM) for Fe^{2+} through change of absorption intensity (absorbance at 457 nm). (b) Detection limit of **1** (10 μM) for Fe^{3+} through change of absorption intensity (absorbance at 457 nm).

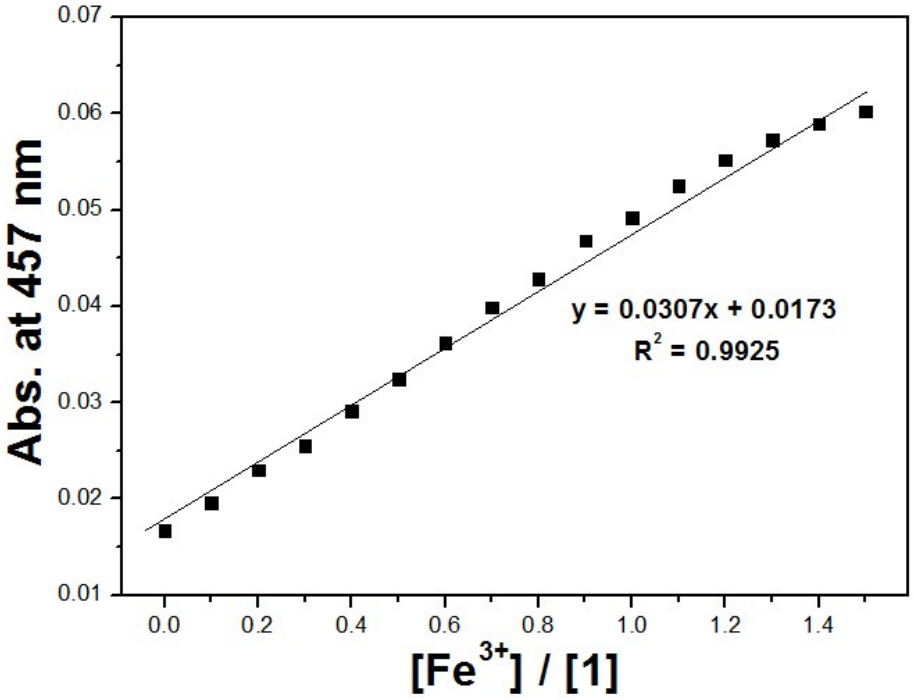

Figure S17. UV-vis spectra (at 457 nm) of **1** as a function of Fe(III) concentration. [**1**] = 10 μM, [Fe(III)] = 0-15.00 μM; Conditions: the sample was conducted in MeOH-buffer solution (9:1, v/v, 10 mM, bis-tris, pH 7.0).